Journal of Catalysis **187,** 419–435 (1999)
Article ID jcat.1999.2603, available online at http://www.idealibrary.com on IDEAL®

Characterization and Reactivity of V_2O_5–MoO_3/TiO_2 De-NO_x SCR Catalysts

Luca Lietti,*,[1] Isabella Nova,* Gianguido Ramis,† Lorenzo Dall'Acqua,‡ Guido Busca,† Elio Giamello,‡ Pio Forzatti,* and Fiorenzo Bregani,§

*Dipartimento di Chimica Industriale ed Ingegneria Chimica "G. Natta", Politecnico di Milano, P.zza L. da Vinci 32, 20133 Milan; †Dipartimento di Ingegneria Chimica e di Processo "G.B.Bonino", Facoltà di Ingegneria, Università di Genova, P.le Kennedy, 16129 Genoa; ‡Dipartimento di Chimica Inorganica, Chimica Fisica e Chimica dei Materiali, Università di Torino, Viale P. Giuria 9, Turin; and §ENEL, Area generazione, Via Reggio Emilia 39, Segrate (MI), Italy

Received April 6, 1999; revised June 18, 1999; accepted June 23, 1999

TiO_2-supported V_2O_5–MoO_3 catalysts, having V and Mo loadings representative of commercial SCR catalysts, are considered in this study. These catalysts are constituted by TiO_2 anatase supporting the V and Mo active components. MoO_3 acts as a "structural" promoter preventing the TiO_2 matrix from sintering upon vanadia addition. The Mo and V oxide are present on the catalyst surface in the form of molybdenylic and vanadylic species, respectively, and the presence of polymeric Mo_xO_y species cannot be excluded. The features of the V and Mo surface oxide species closely resemble those observed over the binary V_2O_5/TiO_2 and MoO_3/TiO_2 catalysts, thus pointing out the vibrational independence of the V and Mo surface vanadyl and molybdenyl oxide species. However, in spite of their structural and vibrational independence, the presence of electronic interactions between the TiO_2-supported V and Mo oxides is also apparent. These interactions may operate via the TiO_2 support or may involve mixed V–Mo surface oxide species who were, however, not observed. The catalyst surface is characterized by strong acidity, probed by NH_3-TPD and FT-IR. Ammonia is coordinatively held over Lewis acid sites (associated with Ti, V, and Mo surface cation species) and is protonated as NH_4^+ ions over Mo–OH or V–OH Brønsted sites. The addition of Mo and V causes the formation of Brønsted sites and of stronger Lewis acid sites, if compared to TiO_2. The V_2O_5–MoO_3/TiO_2 catalysts are very active in the reduction of NO by NH_3, and exhibit a higher reactivity with respect to the corresponding binary V_2O_5/TiO_2 and MoO_3/TiO_2 samples. Calculations show that the reactivity of V and/or Mo in the ternary catalysts is higher than that measured over V_2O_5/TiO_2 and MoO_3/TiO_2 having the same V and Mo loading: hence it is suggested that a synergism operates in the SCR reaction between the V and Mo surface oxide species. Accordingly in these catalysts molybdenum also acts as a "chemical" promoter for the SCR reaction. On the basis of the characterization data, it is suggested that the observed synergism in the SCR reaction is related to the existence of the V–Mo electronic interactions. This picture closely resembles that obtained in the case of the analogous V_2O_5–WO_3/TiO_2 system and indicates that the effects of the addition of WO_3 and MoO_3 to V_2O_5/TiO_2 are similar, both oxides acting as "chemical" promoters besides playing a "structural" function as well. However the V_2O_5–MoO_3/TiO_2 samples show higher formation of N_2O and lower NO conversions at high temperatures: these differences are possibly associated with the different electronic characteristics of Mo compared to W and to their higher reactivity in the ammonia oxidation reactions. It is found that water addition in the feed improves the catalyst performance in that it preserves high NO conversions and high N_2 selectivities at high temperatures: this is due to its strong inhibiting effect on the ammonia oxidation reactions occurring simultaneously with the SCR reactions.

Key Words: **selective catalytic reduction of NO_x; V_2O_5–MoO_3/TiO_2 catalysts.**

INTRODUCTION

The Selective Catalytic Reduction (SCR) of NO_x by NH_3 is to date the best developed and most widespread method for NO_x removal from stationary sources (1–3). The process is based on a catalytic reaction between NO contained in the flue gases and injected NH_3 to produce water and nitrogen according to the following stoichiometry:

$$4\,NO + 4\,NH_3 + O_2 \rightarrow 4\,N_2 + 6\,H_2O. \qquad [1]$$

Commercial SCR monolith catalysts are made up by an anatase TiO_2 carrier that supports the active components, i.e., vanadium pentoxide and tungsten (or molybdenum) trioxide. Vanadia is active in the reduction of NO_x but also in the undesired oxidation of SO_2 to SO_3; accordingly the V_2O_5 content is generally low (0.3–1.5% w/w). WO_3 is employed in much larger amounts (nearby 10% w/w), and it acts as both a "chemical" and a "structural" promoter; i.e., it increases the reactivity of V_2O_5/TiO_2 catalysts by enlarging the temperature window of the SCR reaction and improves the mechanical, structural, and morphological properties of the catalysts (4–6). Catalysts containing MoO_3

[1] Corresponding author. Fax: -02-70638173. E-mail: luca.lietti@polimi.it.

0021-9517/99 $30.00

instead of WO_3 are also employed in industrial practice (7, 8). In these catalysts, WO_3 is replaced by a similar amount of MoO_3 on a molar basis: they have been reported to be less active than the analogous V_2O_5–WO_3/TiO_2 samples, but more tolerant to poisoning by As compounds (7, 8).

Detailed investigations on the physico-chemical characteristics and catalytic behavior of V_2O_5–MoO_3/TiO_2 catalysts in the SCR reaction are still scarce in the literature. In particular, the role of molybdenum oxide in the activity and structural and morphological characteristics of the MoO_3-based catalysts has not completely clarified to date. For these reasons, an extensive investigation has been undertaken in our laboratories, aiming at a better understanding of the reactivity and chemico-physical properties of this catalytic system. As a first part of this study, binary MoO_3/TiO_2 model catalysts have been prepared, characterized, and tested in the SCR reaction (9). It has been found that for submonolayer samples the structural and morphological characteristics of the TiO_2 support are not significantly modified upon MoO_3 addition. Mo oxide is present on the TiO_2 surface in the form of isolated molybdenyl surface species for submonolayer coverages, whereas crystalline MoO_3 is formed for molybdenum loadings exceeding the monolayer capacity of the support. The MoO_3/TiO_2 samples are active in the SCR reaction, but poorly selective due to the formation of significant amounts of N_2O. In the present study, the investigation has been extended to the ternary V_2O_5–MoO_3/TiO_2 system: accordingly, model V_2O_5–MoO_3/TiO_2 catalysts with MoO_3 content near 6% w/w and with V_2O_5 loadings in the range 0–2.3% w/w (i.e., of interest for SCR applications) have been prepared and characterized by means of different chemico-physical techniques including surface area and pore size distribution measurements, XRD, FT-IR, FT-Laser Raman, Electron Paramagnetic Resonance (EPR), and NH_3-TPD. The reactivity in the SCR reaction of the samples has also been investigated, and the obtained results are compared with those for V_2O_5–WO_3/TiO_2 reference catalysts having similar composition and investigated in previous papers (5, 6).

METHODS

Catalyst Preparation

TiO_2-supported V_2O_5–MoO_3 catalysts with different vanadia contents and with a nominal MoO_3 content of 6% w/w were prepared by the incipient wetness method. The Mo loading has been selected since it roughly corresponds to that of commercial catalysts and also corresponds, on a molar basis, to the WO_3 content of typical commercial V_2O_5–WO_3/TiO_2 catalysts ($WO_3 \approx 9\%$ w/w) (6).

A home-made titania support in the anatase form was used as support material, prepared by neutralization at constant pH (near 7) of Ti-tetrachloride ($TiCl_4$) with an NH_4OH solution. The TiO_2 precursor was then washed, dried at 383 K overnight, and calcined for 4 h at 823 K.

A MoO_3/TiO_2 catalyst with MoO_3 loading of 6% by weight was then prepared by impregnating the TiO_2 support with an aqueous solution of ammonium heptamolybdate (Carlo Erba RPE) complexed with citric acid (J.T. Baker). The resulting precursor was dried at 383 K overnight and calcined at 823 K for 3 h. Vanadium was added to the MoO_3/TiO_2 binary system by impregnation, starting from a water solution of ammonium metavanadate and oxalic acid, followed by drying and calcination at 823 K for 2 h. Samples with V_2O_5 loadings of 0.4, 0.8, 1.5, and 2.3% w/w were prepared.

In the following, catalysts are denoted as $V_2O_5(x)$–$MoO_3(6)/TiO_2$, where the numbers in the brackets represent the % w/w metal oxide loading.

Catalyst Characterization

Surface area was measured by N_2 adsorption at 77 K with the BET method using a Carlo Erba Sorptomatic 1900 Series instrument. Pore size distribution measurements were obtained by N_2 adsorption–desorption at 77 K with the same apparatus used for surface area measurements and by the mercury penetration method using a Carlo Erba Porosimeter 2000 Series instrument.

Powder X-ray diffraction analyses were performed with a Philips vertical goniometer PW 1050/70 and Ni-filtered Cu $K\alpha$ radiation. XRD spectra were used to estimate the mean crystal size of the TiO_2 crystallites (d_{cryst}) by using the Scherrer equation.

The FT-IR spectra were recorded with Nicolet Magna 750 and 5ZDX Fourier Transform spectrometers at R.T. (4 cm^{-1} resolution). The powders were pressed into self-supporting disks and activated by outgassing at 623 K before adsorption experiments. The skeletal spectra in the region 2000–400 cm^{-1} were recorded with KBr-pressed disks. Ammonia adsorbed on the catalyst surface was taken from commercial cylinders from Sapio (Italy).

FT-Raman spectra were recorded using a Brucker RFS100 (Nd:YAG laser) instrument.

The EPR spectra were obtained with a Varian E 109 Spectrometer operating between 9.2 and 9.5 GHz microwave frequency and with a field of modulation of 100 kHz; the spectrometer was equipped with a dual cavity and connected to a personal computer for spectra recording and elaboration. A weighted amount of the calcined catalyst was introduced, for all experiments, in a quartz EPR cell connected to a vacuum manifold which was evacuated at room temperature to allow EPR spectra recording in the absence of oxygen. A quantitative analysis of the spectra was performed based on the comparisons between the integrated intensities of each spectrum with that of standard

$VOSO_4/K_2SO_4$ samples according to the method proposed by Dyrek and co-workers (10).

NH_3-TPD experiments were performed with the same apparatus used for catalytic activity runs (see below). In a typical experiment, 160 mg catalyst is oxidized in He + 20% O_2 at 773 K for 1 h, cooled down at 313 K under the same atmosphere, purged with He, and then saturated at 313 K for 20 min with a stream of NH_3 (2000 ppm) in He (total flow rate = 120 cm^3/min (STP)). At the end of the saturation procedure, pure He is flowed over the catalyst sample at 313 K for 30 min to remove weakly adsorbed ammonia. Finally the TPD spectrum is recorded by heating the catalyst in pure He (120 cm^3/min) up 773 K at 15 K/min.

Reactivity Measurements

Catalytic activity measurements have been performed in a quartz tubular fixed-bed microreactor (i.d. = 7 mm) operating at atmospheric pressure and inserted into an electric furnace. The temperature of the catalyst was measured and controlled by means of a K-type thermocouple (o.d. = 0.5 mm) directly immersed in the catalyst bed. In a typical run 160 mg (100–150 mesh) of catalyst were used and a stream of NH_3 (800 ppm) + NO (800 ppm) + O_2 (9000 ppm) + Ar (1500 ppm, internal standard) in He (total flow rate = 120 cm^3/min (STP)) was fed to the reactor maintained at a desired temperature value. Each reaction temperature was maintained for at least 2 h. For the analysis of the exiting gases, the reactor outlet was connected in a parallel arrangement to both a quadrupole mass detector (Balzers QMS 200) and a gas chromatograph (HP 6890) equipped with a Porapak Q and 5 Å molecular sieve capillary columns (Chromopack) connected to thermal conductivity detectors. The following mass-to-charge ratios were used to monitor the concentrations of products and reactants: 17 (NH_3), 18 (H_2O), 28 (N_2), 30 (NO), 32 (O_2), 44 (N_2O), and 46 (NO_2). The data were quantitatively analyzed by taking into account the response factors and the fragmentation patterns of the various species experimentally determined. A quantitative evaluation of N_2, O_2 + Ar, N_2O, and H_2O was also obtained by GC, and results compare well with mass-spectrometer data. N-balances, calculated on the gas exiting the reactor, always closed within ±5%, being typically lower than ±3%.

The reactivity of the catalysts was also investigated under transient conditions. In this case Temperature Programmed Reaction (TPRn) experiments of $NH_3 + O_2$ and of $NH_3 + NO + O_2$ were performed in the same apparatus used for steady-state catalytic activity experiments. In a typical TPRn experiment, a flow of NH_3 (800 ppm) + 2% v/v O_2 in He or of NH_3 (800 ppm) + NO (800 ppm) + 2% v/v O_2 in He (total flow rate = 120 cm^3/min (STP)) was fed to the catalyst kept at 313 K. When the mass spectrometer signals had stabilized (typically within 30 min), the catalyst was heated up to 773 K at 15 K/min while the flow rate was held constant and the concentrations of the various species were monitored.

RESULTS

XRD and Morphology

The effect of the vanadia loading on the catalysts' structural and morphological properties was investigated first. Table 1 reports the phase composition identified by XRD, the mean crystal size of the TiO_2 crystallites (d_{cryst}), the surface area (S_a), the pore volume (V_p), the mean pore radius (r_p), and the V_2O_5 and MoO_3 surface coverage (θ_V and θ_{Mo}, respectively) calculated from the nominal V_2O_5 and MoO_3 loading and the specific surface area of the sample. In this calculation a monolayer capacity of 0.145% w/w for V_2O_5/m^2 (11) and of 0.12% w/w for MoO_3/m^2 (12, 13) has been assumed. The overall V + Mo surface coverage has been estimated by simply summing those of V and Mo. As reported in Table 1, the theoretical V + Mo monolayer coverage is reached only in the sample with the highest V_2O_5 loading.

For all the samples, the only phase detected by XRD is the anatase polymorphic form of TiO_2, and no significant differences are observed in the crystallite dimensions of anatase on increasing the V_2O_5 content. No diffraction lines assignable to crystalline V_2O_5 or MoO_3 are detected: the absence of these bulk phases in the XRD patterns implies that for these samples the molybdenum and vanadium oxides are present in either a noncrystalline state or as small crystallites (less than 4 nm in diameter).

The morphological characteristics of the samples are slightly modified upon V_2O_5 addition in the range 0–2.3% w/w: the BET surface area of the catalysts decreases progressively from 79 down to 64 m^2/g, whereas the pore volume and the mean pore radius are not significantly affected by vanadia addition and are in the range 0.27–0.31 cc/g and 70–100 Å, respectively.

TABLE 1

Structural and Morphological Data of $V_2O_5(x)$–$MoO_3(6)/TiO_2$ Samples (x = 0–2.3% w/w), Calcined at 823 K

V_2O_5 (% w/w)	0	0.4	0.8	1.5	2.3
Phase	Anatase	Anatase	Anatase	Anatase	Anatase
d_{cryst} (Å)	150–160	160–165	160–170	160–165	165–170
S_a (m^2/g)	79	72	70[a]	68[b]	64
V_p (cc/g)	0.31	0.30	0.30	0.27	0.27
r_p (Å)	60–70	80–90	80–90	90–100	90–100
θ_V	0	0.04	0.08	0.15	0.25
θ_{Mo}	0.63	0.69	0.72	0.73	0.78
θ_{V+Mo}	0.63	0.73	0.80	0.88	1.03
θ_{Ti}	0.37	0.27	0.20	0.12	0

[a] Sixty-five m^2/g for $V_2O_5(0.8)/TiO_2$.
[b] Sixty-four m^2/g for $V_2O_5(1.5)/TiO_2$.

Reference binary V_2O_5/TiO_2 samples with vanadia loading of 0.8 and 1.5% w/w have also been prepared and characterized for the purpose of comparison. These samples present a BET surface area of 65 and 64 m^2/g and a pore volume of 0.29 and 0.32 cc/g, respectively. Only the anatase polymorphic form of TiO_2 has been detected by XRD in both cases, with a mean dimension of the TiO_2 crystallites near 160 Å. A comparison of the surface areas of these samples with those of the MoO_3-containing catalysts having the same V_2O_5 loading (65 vs 70 m^2/g for the samples with $V_2O_5 = 0.8$ and 64 vs 68 m^2/g for $V_2O_5 = 1.5$) indicates that the presence of Mo on the catalyst surface inhibits the sintering of the TiO_2 matrix, which on the other hand is favored by the presence of vanadia (6).

Spectroscopic Studies

Information concerning the structural and vibrational characteristics of molybdenum and vanadium oxide on the TiO_2 surface are provided by the spectroscopic analysis (FT-IR, FT-Raman, and EPR).

FT-Raman. In Fig. 1 the FT-Raman spectra of the $MoO_3(6)/TiO_2$ sample and of selected $V_2O_5(x)$–$MoO_3(6)/TiO_2$ ternary catalysts are shown as such. The spectrum of $MoO_3(6)/TiO_2$ (trace a) shows five peaks at 639, 515, 396, 195, and 143 cm^{-1}, due to the six Raman active fundamentals of anatase, two of which are superimposed at 515 cm^{-1} (14). Neither rutile nor brookite are present as impurities, thus confirming XRD data. Furthermore, no evidence of bulk MoO_3 bands at 994 and 818 cm^{-1} in the Raman spectrum are found (15). Additional weak scattering is observed in the spectral region 1000–900 cm^{-1}, due to molybdenum oxide species. The spectra of the ternary catalysts (traces b–d) again show the peaks of anatase and the weak scattering near 970 cm^{-1} due to the molybdenum oxide species, but the intensity of the peaks is weakened by increasing the vanadium amount. No additional scattering in the region 1000–800 cm^{-1} due to V–O stretching of vanadyl or vanadate species is detected. The decrease in the anatase peak intensities in supported metal oxides has also been reported in the case of V_2O_5/TiO_2 (16), MoO_3/TiO_2 (17), Cu/TiO_2 (17), and SiO_2/TiO_2 (18) catalysts, and has been observed by some of us in V_2O_5–WO_3/TiO_2 SCR catalysts as well (6). This effect has been related to three different factors, increased disorder of the surface, increased absorption of the exciting radiation, and more complex solid-state phenomena like phonon–plasmon couplings (6).

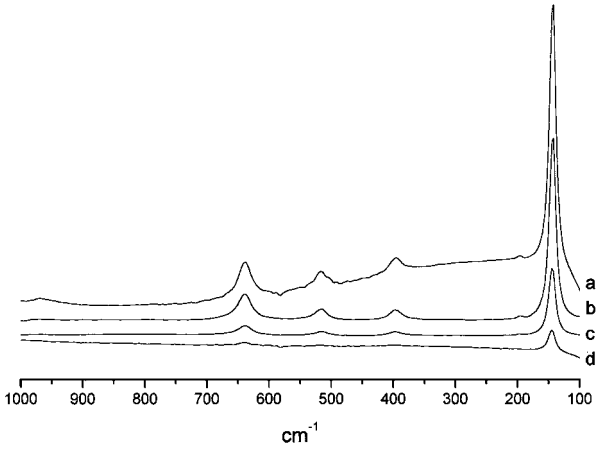

FIG. 1. FT-Laser Raman spectra of $MoO_3(6)/TiO_2$ (a), $V_2O_5(0.8)$–$MoO_3(6)/TiO_2$ (b), $V_2O_5(1.5)$–$MoO_3(6)/TiO_2$ (c), and $V_2O_5(2.3)$–$MoO_3(6)/TiO_2$ (d) catalysts.

FT-IR. The FT-IR spectra (KBr pressed disks) of the $MoO_3(6)/TiO_2$ sample and of $V_2O_5(x)$–$MoO_3(6)/TiO_2$ ternary catalysts, not reported for brevity, show a strong absorption in the region 800–500 cm^{-1} typical of TiO_2 anatase (17) and a shoulder near 960 cm^{-1} due to the molydenum oxide species. Vanadium-containing catalysts show the same spectral feature, although the presence of a weak shoulder near 1000 cm^{-1} could be not excluded. According to previous data (19, 20) the weak band in the range 970–930 cm^{-1} is assigned to the terminal Mo=O stretching of the hydrated form of the surface molybdenyl species like $[O_3Mo{=}O]^{2-}$. This band, broad and weak under wet conditions, shifts to higher frequencies under dry conditions, giving rise to a sharp band near 1000 cm^{-1}, with the first overtone near 1980 cm^{-1} (see below). In line with the Raman spectra, no evidence of bulk MoO_3 bands near 960 cm^{-1} with complex overtones at 1955, 1925, and 1833 cm^{-1} (21) are found, while we cannot exclude the presence of a symmetric tetrahedral molybdate ion $[MoO_4]^{2-}$ whose symmetric stretching mode typically falls near 900 cm^{-1} and could be responsible of the broadening towards the lower frequency of the band at 970 cm^{-1}. Finally, it is worthy of note that no direct evidence has been obtained for the existence of polymeric Mo_xO_y species, whose presence, however, cannot be excluded on the basis of the present data.

The FT-IR features of the surface V and Mo oxide species have also been investigated under dry conditions. Since upon adsorption of molecules like ammonia (or water) the bands due to the stretching modes of Mo=O and V=O broaden and shift to lower frequencies, it is possible to point out these bands as negative absorptions by subtracting the spectrum of the NH_3-covered sample from that of the pure powder sample. The difference spectra (overtone region) obtained in the case of the $MoO_3(6)/TiO_2$ sample and of the $V_2O_5(x)$–$MoO_3(6)/TiO_2$ ternary catalysts are reported in Fig. 2. In the case of the $V_2O_5(1.5)/TiO_2$ and $MoO_3(6)/TiO_2$ binary reference catalysts (traces a and e of Fig. 2, respectively), the negative bands due to the first overtone of the fundamental Mo=O and V=O stretching mode of vanadyls and molybdenils species are clearly detectable, according to previous data, at 1975 (19) and 2048 cm^{-1} (22, 23), respectively.

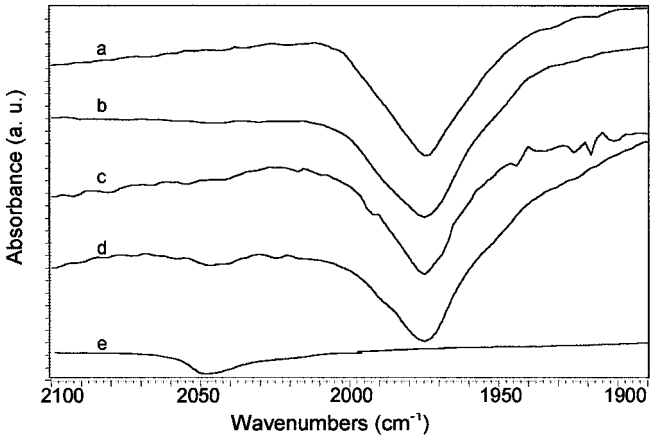

FIG. 2. FT-IR spectra (dry conditions) of $MoO_3(6)/TiO_2$ (a), $V_2O_5(0.4)$–$MoO_3(6)/TiO_2$ (b), $V_2O_5(0.8)$–$MoO_3(6)/TiO_2$ (c), $V_2O_5(1.5)$–$MoO_3(6)/TiO_2$ (d), and $V_2O_5(1.5)/TiO_2$ (e) catalysts. Overtone region, spectrum of the ammonia-covered sample subtracted.

In the case of the ternary $V_2O_5(x)$–$MoO_3(6)/TiO_2$ samples (traces b–d), the band of the first overtone of the fundamental Mo=O stretching mode of molybdenyls species is split in two components: indeed a main component is evident at 1976 cm^{-1}, as in the binary $MoO_3(6)/TiO_2$ reference sample, and a weak shoulder is detected at 1995 cm^{-1}. A negative band is also visible at 2045 cm^{-1} in the case of the $V_2O_5(1.5)$–$MoO_3(6)/TiO_2$ sample (trace d): this band is due to the first overtone of the V=O stretching mode, that is detectable only in the spectrum of the sample with the highest amount of vanadium. The corresponding fundamental mode, not reported in the figure, is also visible near 1000 cm^{-1}.

EPR. Among the various paramagnetic ions potentially present at the surface of the investigated V_2O_5–MoO_3/TiO_2 samples, only Mo(V) and V(IV) have been observed. Both Mo(V) and V(IV) are d^1 species whose resonance is expected to take place in the same region of the magnetic field, i.e., at g values lower than the free spin value g_e ($g_e > g_\perp > g_\parallel$ for tetragonally distorted octahedral or square pyramidal systems). However, the individual spectral profiles of Mo(V) and V(IV) EPR spectra are different in that Mo(V) exhibits a relatively weak hyperfine sextet centered on the $g_\perp$ component, due to the interaction between the unpaired electron and the $I = 5/2$ ^{95}Mo and ^{97}Mo nuclei, whose natural abundance is 15.8 and 9.6%, respectively. The spectral profile of V(IV) is more complex in that both g components are split in eight lines due to the interaction with the $I = 7/2$ nucleus of ^{51}V, whose abundance is 100%. Very few EPR characterizations of TiO_2 supported V_2O_5/MoO_3 systems are available in the literature (24), and most published work concerns binary systems such as V_2O_5/TiO_2 (25–32) and MoO_3/TiO_2 (9, 33) or ternary systems like V_2O_5–WO_3/TiO_2 (6, 34). EPR investigations of the supported oxides mentioned above (in experimental conditions close to those employed in the present work) always revealed the presence of a single paramagnetic species only (V(IV) or Mo(V) according to the case).

V_2O_5–MoO_3/TiO_2 samples calcined at 823 K are yellow (0.4 wt% V_2O_5 loading) or brownish for higher V_2O_5 content (0.8–1.5 wt%). The EPR spectrum of the calcined $V_2O_5(0.4)$–$MoO_3(6)/TiO_2$ sample is reported in Fig. 3 (spectrum a). The spectrum is due to V(IV) species and confirms what was already found for V_2O_5–WO_3/TiO_2 (6, 34), i.e., the propensity of a small fraction of the supported vanadium to be in the partially reduced V(IV) state even after calcination of the solid at high temperature. Upon evacuation for 1 h at 423 K, a complex and more intense spectrum is obtained (spectrum b of Fig. 3). The spectrum can be interpreted as the superposition of a strong Mo(V) signal to the V(IV) features observed for the calcined sample (spectrum a). Both the parallel and the perpendicular Mo(V) components are clearly visible in spectrum b in which the intensity of the V(IV) features are the same as in spectrum a, despite

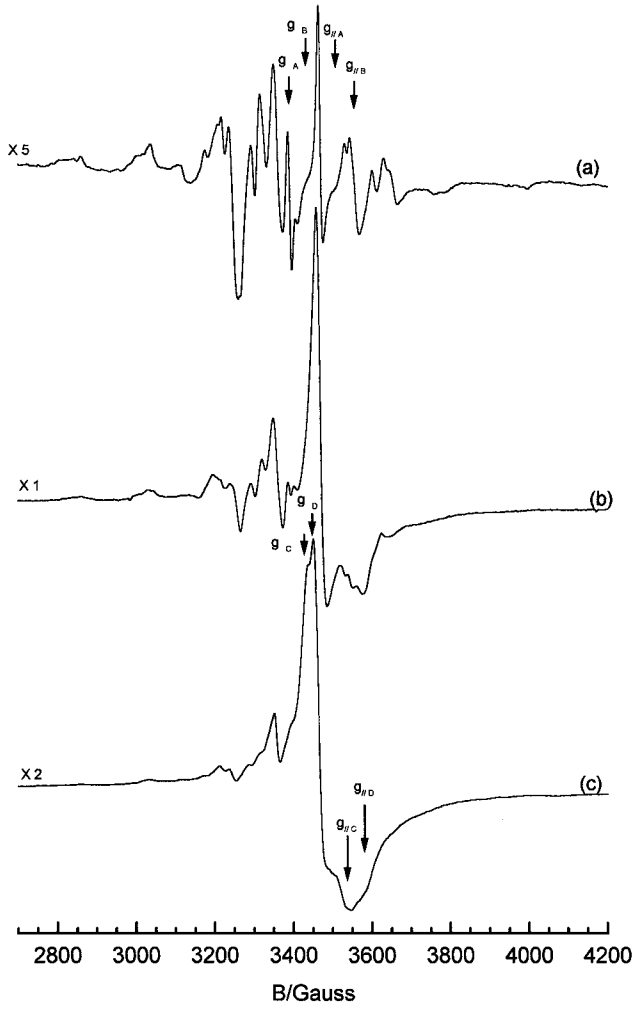

FIG. 3. EPR spectra of $V_2O_5(0.4)$–$MoO_3(6)/TiO_2$ calcined at 823 K and outgassed at R.T. (a) and 423 (b) and 623 K (c).

TABLE 2

Spin–Hamiltonian Parameters for Vanadylic and Molibdenylic Species

Species	Nature	$g_{\parallel}$	$g_{\perp}$	g_{iso}	$A_{\parallel}$	$A_{\perp}$	A_{iso}
A	VO^{2+}	1.9135	1.9825	1.9595	195.2	72.3	113.3
B	VO^{2+}	1.8967	1.9778	1.9500	195.7	69.2	111.4
C	MoO^{3+}	1.9042	1.9567	1.9392	—	41.0	—
D	MoO^{3+}	1.8864	1.9467	1.9266	—	43.0	—

an apparent reduction due to the different amplification of the two spectra. Evacuation at 623 K for 1 h brings about a dramatic decrease of V(IV) signal (spectrum c), while that of Mo(V) is less affected by the treatment.

The features of the V(IV) species present on the ternary $V_2O_5(0.4)MoO_3(6)/TiO_2$ catalyst evacuated after calcination at R.T. and at 423 K (spectra a and b of Fig. 3) are due to the contribution of two V(IV) species, slightly differing in their coordinative environment. The spin–Hamiltonian parameters of the two species (A and B) have been derived by computer simulation and are reported in Table 2. Comparison with literature data (10, 25–32) suggests that all the V(IV) species present in the spectra are typical surface vanadylic ions $(VO)^{2+}$ in axial symmetry.

The features of Mo(V) species have been derived by a simulation of spectrum c of Fig. 3, where only the features of Mo(V) species are evident. Like for vanadium, the spectrum is determined again by the presence of two distinct but similar species (C and D in Table 2). These species are strictly similar to those observed in the case of MoO_3/TiO_2 catalysts (9) and correspond to surface molybdenyl ions $(MoO)^{3+}$ in axial symmetry (24).

The described thermal treatment was performed for all samples containing different V_2O_5 percentages, always obtaining the same results in term of the spectral parameters of V(IV) and Mo(V) species. However, on increasing the V_2O_5 loading, higher temperatures are necessary to obtain the decrease of the intensity of the vanadium signal and the appearance of the molybdenum profile, as shown in Fig. 4 for the $V_2O_5(1.5)$–$MoO_3(6)/TiO_2$ catalyst taken as an example. Due to the higher V loading of this sample, the signals are broader in all conditions and the spectra result less resolved than those shown in Fig. 3. The line broadening, observed in terms of a strong base line drift, very likely involves both V(IV) and Mo(V) signals, thus indicating a sort of more pronounced mutual magnetic interaction between supported paramagnetic species. This interaction could be, in principle, both between similar species (Mo(V)–Mo(V), V(IV)–V(IV)) and between different species (V(IV)–Mo(V)).

The samples with different vanadium loadings also differ in the whole signal intensities, i.e., in the amount of reduced paramagnetic ions present at the surface. A quantitative analysis of the EPR spectra indicated that for all the samples the intensity of the EPR signal increases with outgassing temperature reaching a maximum at 423 K. Then the intensity of the EPR signals remains constant for the $V_2O_5(0.4)$–MoO_3/TiO_2 catalysts up 623 K while it decreases for the other samples. The $\%[V(IV)+Mo(V)]/[V+Mo]_{total}$ ratio, i.e., the fraction of reduced EPR active surface species, ranges from 7 to 11.5% w/w for the samples treated at 423 K. The decrease of the total intensity brought on by increasing the temperature over 423 K indicates that the reduction of the samples at these temperatures involves the formation of species at lower oxidation number than V(IV) and Mo(V) which are not EPR visible.

On increasing the V_2O_5 percentage, the reducibility of the whole supported system also increases. In particular, V(IV) reduction occurring in the range 423–623 K is more pronounced in the case of the $V_2O_5(1.5)$–$MoO_3(6)/TiO_2$ catalyst (Fig. 4, spectra b–c) than in the case of the low loading sample (Fig. 3, spectra b–c).

The quantitative analysis clearly indicates that the one electron reduction for pentavalent V species ($V(V)+e^- \rightarrow V(IV)$) occurs before the analogous reduction of molybdenum ($Mo(VI)+e^- \rightarrow Mo(V)$) or, in other words,

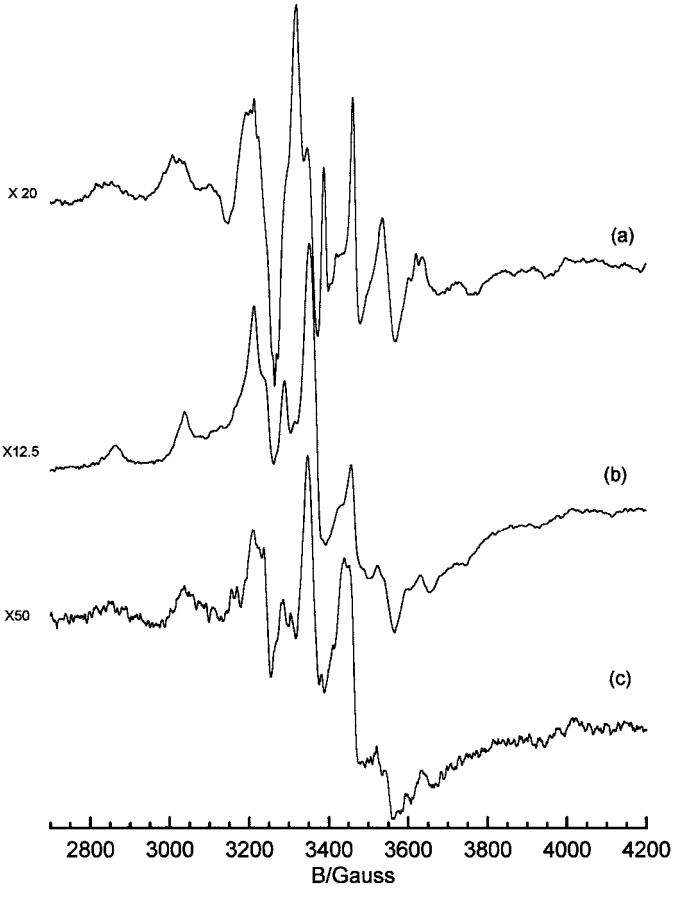

FIG. 4. EPR spectra of $V_2O_5(1.5)$–$MoO_3(6)/TiO_2$ calcined at 823 K and outgassed at R.T. (a) and 423 (b) and 623 K (c).

that the reducibility of the supported vanadium phase is higher than that of the molybdenum phase, at least in the case of the lower loading $V_2O_5(0.4)$–MoO_3/TiO_2 sample, which exhibits the more reduced EPR spectra (Fig. 3). This is not surprising and is in agreement with the standard reduction potentials in solution of the two semi-reactions reported above (0.99 and 0.48 V, respectively) (35) and with the results reported by Busca and Marchetti (24).

Interaction of Ammonia with the Catalyst Surface

Temperature Programmed Desorption (TPD) of ammonia. Temperature Programmed Desorption experiments of NH_3 (NH_3-TPD) have been performed with the aim of investigating the acid characteristics of the catalysts. Figure 5 shows the results of the ammonia TPD runs performed over the $V_2O_5(x)$–$MoO_3(6)/TiO_2$ catalysts ($x = 0$, 0.8, and 1.5% w/w).

In all cases the spectra show similar features, with ammonia and water as the main desorption products along with minor amounts of N_2 observed at high temperature. For the $MoO_3(6)/TiO_2$ catalyst, the evolution of ammonia occurs with a broad shape in a wide temperature range (350–720 K), showing a maximum near 420 K. This clearly points out the presence of several NH_3 adsorbed species with different thermal stability. As already discussed in (9), the nonnegligible amount of water desorbed in the TPD experiments in the range 350–600 K is likely related to the presence of water impurities in the NH_3 feed and/or to surface dehydroxylation. The first effect is possibly of minor importance due to both the expected low amounts of water impurities and the lower basicity of water with respect to ammonia, which is known to displace H_2O from the catalyst acid sites (23). On the other hand, it is likely that surface dehydroxylation of a catalyst already calcined at high temperature is favored by the presence of ammonia, which is a vehicle for proton migration (9). The small water peak observed at higher temperatures, near 650 K, is related to the occurrence of the ammonia oxidation process, as indeed confirmed by the production of small amounts of nitrogen that is observed to desorb in the same temperature range.

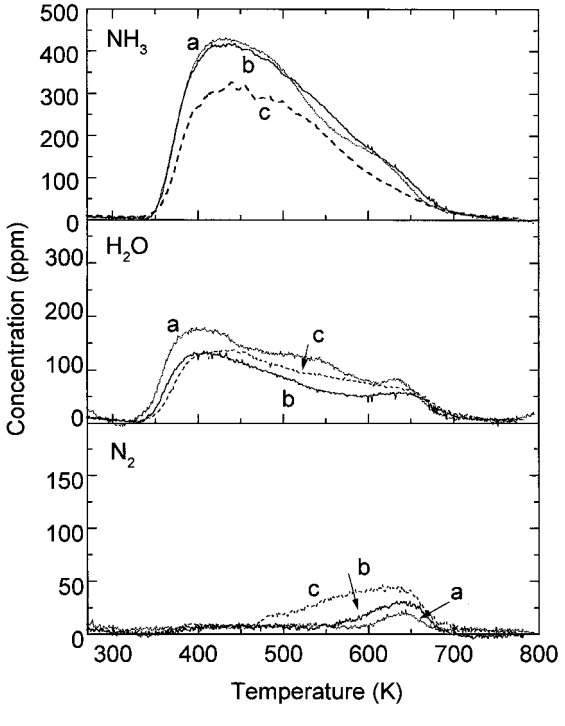

FIG. 5. NH_3-TPD spectra of $MoO_3(6)/TiO_2$ (a), $V_2O_5(0.8)$–$MoO_3(6)/TiO_2$ (b), and $V_2O_5(1.5)$–$MoO_3(6)/TiO_2$ (c) catalysts.

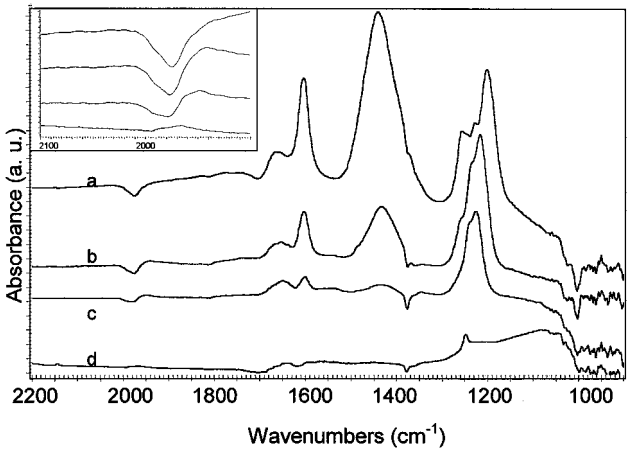

FIG. 6. FT-IR spectra of the adsorbed species arising on $V_2O_5(0.4)$–$MoO_3(6)/TiO_2$ after adsorption of NH_3 and subsequent outgassing at R.T. (a) and 423 (b), 523 (c), and 623 K (d). The spectra of the activated sample have been subtracted. The insert in the figure shows the region of the first overtone of the V=O and Mo=O stretching.

Upon addition of V_2O_5 to the $MoO_3(6)/TiO_2$ catalyst (traces b–c), the features of the NH_3-TPD are only slightly affected: a slight reduction of the area of the NH_3 desorption peak is observed, along with an increase in the formation of nitrogen. This is in line with the promoting effect of vanadium in the oxidation of ammonia (36).

FT-IR study of ammonia adsorption. The interaction of NH_3 with the catalyst surface has also been investigated by FT-IR. Figure 6 shows the FT-IR spectra obtained upon adsorption of ammonia at R.T. over the $V_2O_5(0.4)$–$MoO_3(6)/TiO_2$ sample and after evacuation at increasing temperature.

In the spectrum recorded after evacuation at R.T. (spectrum a), the sharp band at 1604 cm^{-1} is due to the asymmetric deformation of ammonia coordinatively held over Lewis acid sites. The corresponding symmetric deformation mode is complex, showing a band with a maximum near 1200 cm^{-1} and shoulders at 1256, 1250, and 1227 cm^{-1}, indicating that different types of Lewis acid sites are present on the surface.

This band progressively shifts at higher frequency and the relative intensities of its components change upon heating (spectra b–d).

The bands observed at 1668 and 1448 cm^{-1} are characteristic of ammonium ions produced by ammonia protonation over MoOH and, eventually, VOH Brønsted acid sites.

Outgassing at progressively higher temperature (spectra c–d) causes the disappearance first of the bands characteristic of the protonated ammonia species and later of those corresponding to the molecularly adsorbed NH_3. This clearly indicates that protonated NH_4^+ species are thermally less stable than molecularly coordinated species.

It is noted that after evacuation at 423 K (spectrum b), two very weak absorption bands are also detectable at 1540 and 1487 cm^{-1}. These bands could be present also in the spectra recorded at lower temperature (see shoulder near 1490 cm^{-1} after evacuation at R.T.), but appear to be more evident when intensities of the bands of symmetric deformation of ammonia and ammonium decrease; moreover they disappear after evacuation at 523 K, indicating that they are reasonably due to intermediate species. Bands at these frequencies have been observed on the surface of other metal transition oxides supported on titania (37) after adsorption of ammonia and hydrazine; several of these catalysts, active both in the SCR of NO_x and in the Selective Catalytic Oxidation (SCO) of ammonia, show these bands very intensely, and their assignment is not clear at the moment. According to the IR spectra of organic (38) and inorganic N-containing compounds (39), we can tentatively propose that the band at 1487 cm^{-1} is due to HNO nitroxyl adsorbed species and the band at 1540 cm^{-1} is due to NH_2 amide group. We cannot exclude the presence of other intermediates on the surface, but, in any case, these bands are likely due to oxidation products of ammonia.

As discussed above, the negative peaks detected in the spectra correspond to absorption observed over the clean surfaces that disappear upon ammonia adsorption. The negative band at 1976 cm^{-1}, with a shoulder at 1995 cm^{-1}, is due to the first overtone, split in two components, of the Mo=O stretching of surface molybdenyl species (insert of Fig. 6). The corresponding fundamental mode is evident near 1000 cm^{-1}. Together with this band a negative weak peak at 1378 cm^{-1} is also observed, which is assigned to sulfate impurities (40) detectable also on the surface of bare TiO_2 support. With outgassing at increasing temperature the intensity of all these negative bands decreases, indicating that the coordinatively unsaturated molybdenil and sulfate surface groups tend to be regenerated. Focusing attention on the Mo=O stretching overtone shown in the insert of Fig. 6, we observe that upon increasing temperature the lower frequency component at 1976 cm^{-1} is restored more quickly than the higher frequency one.

It is interesting to focus attention on the bands relating to the symmetric deformation of chemisorbed ammonia (spectrum a of Fig. 6) that are sensitive to the strength of the surface acid site and shift towards higher frequency by interaction with increasing acidity of the Lewis sites. This absorption mode appears well split into three components at 1256, 1227, and 1200 (stronger) cm^{-1} with a shoulder at 1250 cm^{-1}. Outgassing at increasing temperature causes a faster disappearance of the components at higher frequency: in fact, after evacuation at 623 K (spectrum d), although weak, only a band at 1250 cm^{-1} is detected. The faster disappearance with temperature of the higher frequency components (representative of the interaction of ammonia with stronger acid sites) may be due to a surface reaction involving ammonia, possibly an oxidation to molecular nitrogen not detectable by FT-IR spectroscopy, and not to the easier desorption of ammonia bonded from more acidic acid sites. As a matter of fact, N_2 formation was observed at temperatures above 600 K during the NH_3-TPD experiments reported above (Fig. 5). Formation of ammonia oxidation products may likely occur via formation of HNO nitroxyl and/or NH_2 amide groups whose presence has been tentatively deduced from the bands at 1487 and 1540 cm^{-1}, respectively.

The spectra recorded after adsorption of ammonia and following evacuation at increasing temperature over the samples with higher vanadia loading present similar features, as shown in the spectra of the sample $V_2O_5(1.5)$–$MoO_3(6)/TiO_2$ taken as an example (see Fig. 7). However, some differences can be observed:

(i) Comparison of the spectra obtained after outgassing at R.T. (traces a of Figs. 6 and 7) shows that the relative intensity of the band at 1448 cm^{-1}, due to symmetric deformation of the ammonium ion, increases with the amount of vanadium in the catalysts with respect to the symmetric deformation of coordinated ammonia on Lewis acid sites, detected near 1605 cm^{-1}.

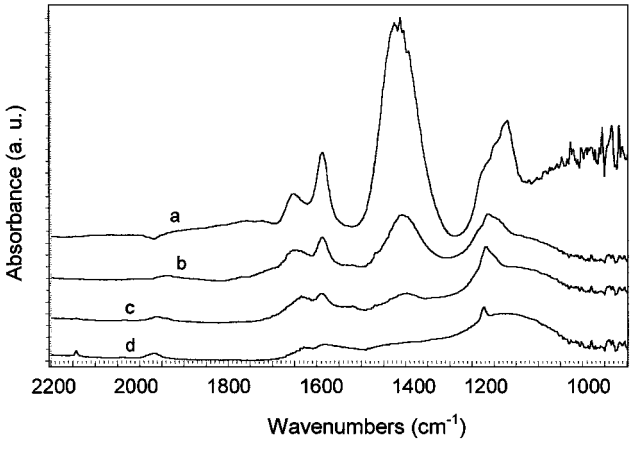

FIG. 7. FT-IR spectra of the adsorbed species arising on $V_2O_5(1.5)$–$MoO_3(6)/TiO_2$ after adsorption of NH_3 and subsequent outgassing at R.T. (a) and 423 (b), 523 (c), and 623 K (d). The spectra of the activated sample have been subtracted.

(ii) In the spectra recorded after evacuation at 523 K (traces b of Figs. 6 and 7), the bands of oxidation ammonia species are always detectable, in particular the band due to amide species, although very weak.

(iii) The negative band at 1378 cm^{-1} is not detectable, indicating that the surface sulfate impurities are no longer present on the surface of the catalysts. This can be interpreted in agreement with the competition, for which evidence was previously reported (41), of sulfate, molybdate, and vanadate species over the support basic sites.

The adsorption of ammonia on binary catalysts and bare support has also been investigated for comparison, but the spectra have not been reported here for brevity. The spectra recorded after adsorption of ammonia and following evacuation at increasing temperature over binary $MoO_3(6)/TiO_2$ and $V_2O_5(1.5)/TiO_2$ catalysts agree well with previously reported data (19, 23). The spectra, showing both ammonium cations and coordinatively bonded molecular ammonia, provide evidence of the presence of both Brønsted and two or three Lewis acid sites of different strengths on the surface of the sample. Molybdenum addition to TiO_2 causes a higher increase of the strength of the Lewis acid sites (as pointed out by a couple of bands at 1252 and 1210 cm^{-1} in the spectrum of $MoO_3(6)/TiO_2$) with respect the vanadium addition (a band near 1200 cm^{-1} with a shoulder at 1240 cm^{-1} is apparent in the spectrum of $V_2O_5(1.5)/TiO_2$). Along similar lines, the loading of vanadium in $MoO_3(6)/TiO_2$ catalyst does not change significantly the strength of the Lewis acid sites, although the formation of a new site, corresponding to the band observed near 1225 cm^{-1} in the spectra of Figs. 6 and 7, could be not excluded.

On the other hand, Brønsted sites are absent on the surface of the pure support, as has been already reported (42). Hence it should be concluded that Brønsted sites originate from the presence of molybdenum or vanadium oxide species on the TiO_2 surface.

Catalytic Activity Measurements

Reactivity in the SCR reaction under dry conditions. The results of the catalytic activity tests performed in the reduction of NO by NH_3 over the V_2O_5–MoO_3/TiO_2 samples having different vanadia content ($V_2O_5 = 0$, 0.8, 1.5% w/w) are shown in Figs. 8A and 8B in terms of NO conversion and N_2 selectivity, respectively. The N_2 selectivity is here defined as $S_{N_2} = [N_2]/([N_2] + [N_2O])$. The results obtained over reference V_2O_5/TiO_2 samples with V_2O_5 loadings of 0.8 and 1.5% w/w have also been reported for comparison purposes (traces d and e, respectively).

Figure 8A shows that all the V_2O_5–MoO_3/TiO_2 samples are active in the SCR reaction and that the reactivity of the catalysts increases on increasing the V_2O_5 loading: the temperature required to achieve 50% NO conversion is progressively lowered from ~570 K down to 470 K on increasing the vanadia loading from 0 to 1.5% w/w (curves a, b, and c, respectively). In the case of the sample with the highest vanadia content, appreciable NO conversions are attained at temperatures as low as 420 K. At the highest investigated temperatures, for all the catalysts the NO conversion decreases due to the occurrence of the NH_3 oxidation reaction: as a matter of fact, the NH_3 conversion (not reported in the figure) is equal to or only slightly higher than that of NO in the whole temperature range, but is always complete in the high temperature region.

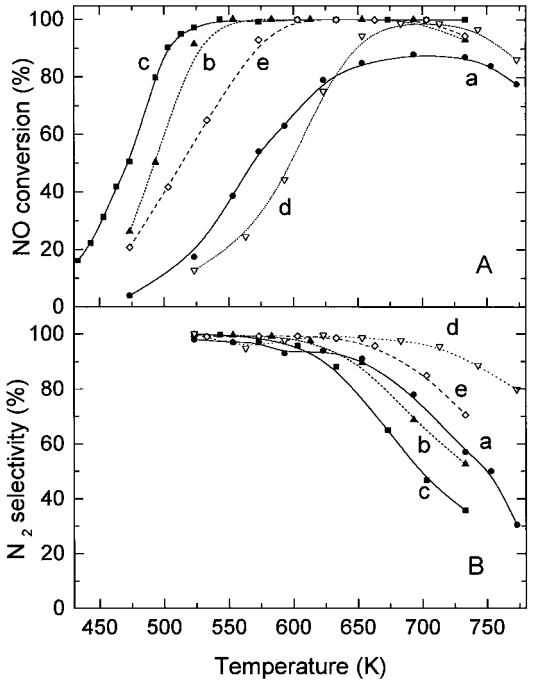

FIG. 8. Results of catalytic activity runs performed over the $V_2O_5(x)$–$MoO_3(6)/TiO_2$ samples and over reference $V_2O_5(x)/TiO_2$ samples. (A) NO conversion vs temperature; (B) N_2 selectivity vs temperature. (a) $MoO_3(6)/TiO_2$; (b) $V_2O_5(0.8)$–$MoO_3(6)/TiO_2$; (c) $V_2O_5(1.5)$–$MoO_3(6)/TiO_2$; (d) $V_2O_5(0.8)/TiO_2$; (e) $V_2O_5(1.5)/TiO_2$.

The N_2 selectivity is nearly complete for all the investigated samples in the low temperature region, but declines at high temperatures due to the formation of N_2O. The decrease of the N_2 selectivity at high temperatures is more evident on the sample with the highest V_2O_5 loading (curve c). It is noted however that in spite of the decrease in the N_2 selectivity with temperature, the temperature window for the reaction (i.e., the temperature range where high NO conversion and high N_2 selectivity are simultaneously achieved) is widened and shifted towards lower temperatures by vanadium addition due to the increased activity of the catalysts in the low temperature region.

The reactivity of the ternary catalysts is significantly higher than that of the corresponding binary samples having the same V loading, as seen by comparing curves d–b and e–c. This effect is particularly evident in the case of the samples with $V_2O_5 = 0.8$% w/w where the NO conversion curve

is shifted 100 K towards lower temperatures. This is a clear indication that the presence of molybdenum increases the activity of V_2O_5/TiO_2 catalysts. Besides, it is worthy of note that the binary V_2O_5/TiO_2 samples show higher N_2 selectivity if compared with the molybdenum-containing catalysts: this may be taken as indication that Mo may contribute to the N_2O formation, as already suggested in previous investigations (9).

To gain a better understanding of the steady-state catalytic activity experiments, the data have been quantitatively analyzed assuming an isothermal plug flow reactor model and a first-order power-law rate equation ($r = k^0 \exp(-E_{act}/RT)C_{NO}$) to estimate k^0 and E_{act}, after the absence of interphase and intraparticle diffusion limitations had been verified with experimental diagnostic criteria. Only the data where almost complete N_2 selectivity was measured have been taken for this kinetic analysis. Comparable values of the activation energy in the range 16.5–19.5 kcal/mol have been calculated for all the samples, except for the $V_2O_5(1.5)/TiO_2$ catalyst for which a slightly lower value of the activation energy (14.1 kcal/mol) has been estimated. These values compare well with those reported in the literature for vanadia/titania based catalysts (43, 44).

Reactivity in the SCR reaction under wet conditions. Since under typical SCR conditions water vapor is contained in huge amounts in the flue gases (~10% v/v), the catalytic behavior of a selected sample (the $V_2O_5(0.8)$–$MoO_3(6)/TiO_2$ catalyst) has also been investigated in the presence of 1% v/v H_2O in the feed. Such a low water content (limited by our experimental apparatus) is representative since it is well known that the H_2O influence on the SCR reaction is strong for low water concentrations and tends to level off at higher H_2O concentrations (1–3). The results of the catalytic activity performed under wet conditions are reported as empty squares in Figs. 9A and 9B (NO conversion and N_2 selectivity, respectively), where they are compared with those obtained under dry conditions. These latter slightly differ from those already reported for the same sample in Fig. 8, possibly due to minor difference in the experimental conditions used in the two cases ($O_2 = 2\%$ v/v vs 9000 ppm). Figure 9 shows that in the low temperature region (i.e., at temperatures below 550 K) the reactivity of the catalyst is only slightly decreased by the presence of steam. On the other hand, a significant effect of H_2O is observed at high temperatures: indeed the presence of water increases the NO conversion and N_2 selectivity at temperatures above 700 K. As a result, the temperature window of the SCR reaction is greatly enlarged towards higher temperatures by water addition, and efficient NO reduction is achieved at temperatures as high as 700 K.

Reactivity in the NH_3 oxidation reaction under dry and wet conditions. The decrease in the NO conversion and N_2 selectivity that is observed at high temperatures under

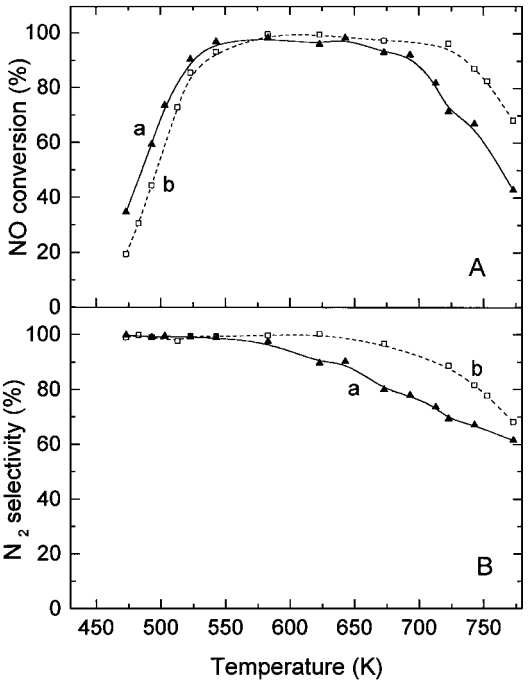

FIG. 9. Results of catalytic activity runs performed over the $V_2O_5(0.8)$–$MoO_3(6)/TiO_2$ sample under dry and wet conditions (empty squares and filled triangles, respectively). (A) NO conversion vs temperature; (B) N_2 selectivity vs temperature.

SCR conditions has been attributed to the occurrence of the NH_3 oxidation reaction (1–3). Accordingly, to better analyze the relevance of such a reaction over the investigated MoO_3-based catalysts, the reactivity of NH_3 in the absence of NO has been investigated under both dry and wet conditions by the Temperature Programmed Reaction (TPRn) method. Figure 10 reports the results obtained in the case of the $V_2O_5(0.8)$–$MoO_3(6)/TiO_2$ catalyst by feeding a stream consisting of NH_3 (800 ppm) + O_2 (2% v/v) in the absence and in the presence of 1% v/v H_2O (traces a and b, respectively). The reactivity of NH_3 in the presence of NO has also been investigated under transient conditions for the sake of comparison and results have been reported in the figure as traces c.

The results obtained in the $NH_3 + NO$ reaction under transient conditions (traces c) closely resemble those secured under steady-state conditions and are already presented in Fig. 9. Indeed NO is consumed starting from 420 K with formation of N_2 and water (not reported in the figure), whereas at higher temperatures, above 670 K, the NO consumption and the N_2 formation decrease, and the formation of huge amounts of N_2O is apparent. The NH_3 concentration trace presents a complex behavior due to its desorption at low temperatures and due to its consumption at high temperatures.

In the case of the $NH_3 + O_2$ reaction performed under dry conditions (traces a), major detected reaction products

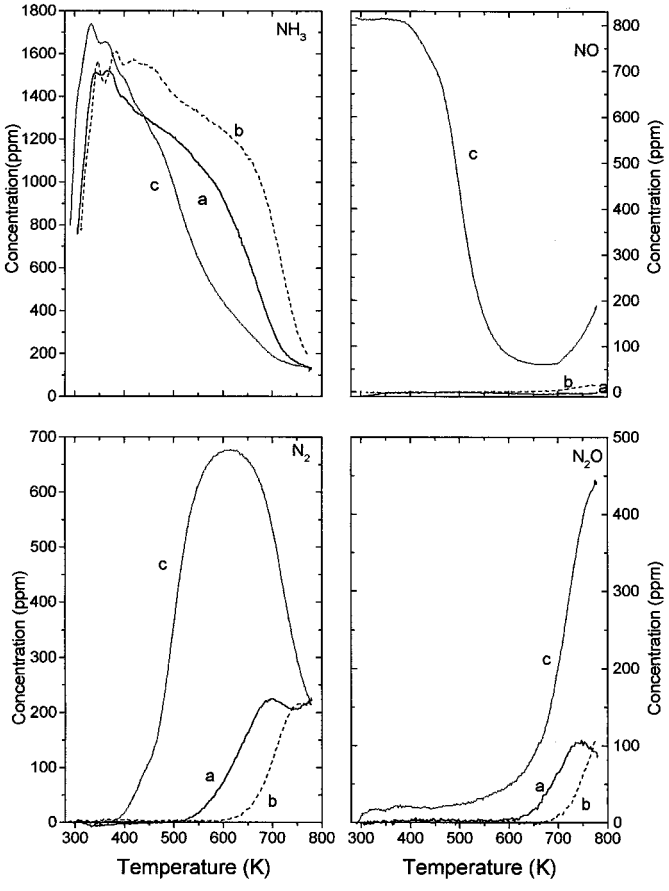

FIG. 10. Results of Temperature Programmed Reaction of $NH_3 + O_2$ (traces a), $NH_3 + O_2 + H_2O$ (traces b), and $NH_3 + NO + O_2$ (traces c) performed over the $V_2O_5(0.8)$–$MoO_3(6)/TiO_2$ sample. Concentration of NH_3, NO, N_2, and N_2O vs temperature.

are N_2 and N_2O, whose formation is apparent at 520 and 620 K, respectively. No formation of significant amounts of NO was observed. Water (not reported in the figure) is also produced along with N_2 and N_2O. It is noted that the greater amounts of N_2O observed during the $NH_3 + NO$ reaction (trace c), if compared to those detected in the case of the NH_3 oxidation reaction (trace a), likely suggest the direct participation of NO in the formation of nitrous oxide. In the presence of water in the feed (curves b of Fig. 10) the occurrence of the ammonia oxidation reaction is significantly hindered, as pointed out by the lower NH_3 consumption and associated N_2 and N_2O formation.

The results reported above clearly indicate that the $V_2O_5(0.8)$–$MoO_3(6)/TiO_2$ catalyst is active in the oxidation of ammonia, leading to the formation of nitrogen and nitrous oxide. The onset of the NH_3 oxidation reaction is evident at higher temperatures if compared to that of the SCR reaction (520 vs 420 K), and is significantly shifted at higher temperatures by water that accordingly strongly inhibits the NH_3 oxidation reaction.

DISCUSSION

Structural and Morphological Characteristics of V_2O_5–MoO_3/TiO_2 Catalysts

In the range of the investigated V and Mo loadings, which are representative of commercial SCR catalysts, our data indicate that the catalysts are monophasic and constituted by TiO_2 anatase supporting the vanadium and molybdenum oxides species. No formation of other crystalline phases has been observed either by XRD or by the more sensitive FT-IR and FT-laser Raman techniques. These data are in line with previous studies indicating that for TiO_2-supported oxides the formation of segregate crystalline phases occurs when the coverage of the surface oxide species exceeds the theoretical monolayer (6, 9).

The morphological characteristics of the starting $MoO_3(6)/TiO_2$ material have not been significantly modified upon addition of vanadia. A comparison with a few V_2O_5/TiO_2 reference catalysts indicates that the presence of Mo on the catalyst surface prevents the TiO_2 matrix sintering process due to vanadia addition. Accordingly Mo oxide acts in these catalysts as a "structural" promoter by preserving the catalyst morphological characteristics upon addition of the active vanadia component, similarly to WO_3 in V_2O_5–WO_3/TiO_2 catalysts (6).

Information concerning the nature of the dispersed V and Mo oxide surface species has been collected by FT-IR, FT-laser Raman, and EPR. For all the investigated $V_2O_5(x)$–$MoO_3(6)/TiO_2$ samples, FT-IR data indicate that molybdenum oxide is present on the TiO_2 surface in the form of molybdenyl species, detected by the Mo=O stretching at 970–930 cm^{-1} (wet conditions) or near 1000 cm^{-1} with the first overtone near 1980 cm^{-1} (dry conditions). The presence of a symmetric tetrahedral molybdate ion $[MoO_4]^{2-}$ cannot be excluded, however, nor can that of polymeric Mo_xO_y species. For what concerns the nature of the V surface oxide species, FT-IR could provide indications only in the case of the sample with high V_2O_5 loading (i.e., $V_2O_5 = 1.5\%$ w/w). In this case the existence of vanadyl species is documented by the presence of the V=O overtone stretching visible at 2045 cm^{-1} (dry conditions). Notably, the position of the bands of the V=O and Mo=O stretching modes of the ternary V_2O_5–MoO_3/TiO_2 catalysts correspond to those observed in binary V_2O_5/TiO_2 and MoO_3/TiO_2 reference catalysts (see Fig. 2): this indicates that these species do not perturb each other from the vibrational point of view. However, in the ternary catalysts, vanadium addition causes the formation of a new weak component at higher frequency in the Mo=O stretching mode characterized by a higher Mo=O bond order. A split of the first overtone of the Mo=O fundamental stretching mode of a surface molybdenyl has been previously observed, and discussed, in molydena–zirconia catalysts for molybdenum loading near to the monolayer (45).

The split of this band is not likely related to the formation of mixed Mo–V oxide species but shows that the overall coordination of the Mo center has an effect at least on the Mo-apical oxygen bond order. On the other hand, the molybdenyl stretching frequency depends on the overall coordination of molybdenum and on the basic strength of its ligands. In conclusion, this can be taken as a measure of the electron-withdrawing character of Mo cations, or, in other words, of their Lewis acidity which is then slightly modified by the presence of vanadium.

Hence, FT-IR data show that the active phases are present on the surface as molybdenyl and vanadyl with one short Mo=O and V=O bond, respectively, and that their primary interaction is with the nucleophilic sites of the TiO_2 support. However, the presence of structural V–Mo interactions cannot be ruled out.

Additional structural information on the surface V and Mo species comes from EPR spectroscopy. The presence of both V(IV) and Mo(V) ions is clearly visible in the EPR spectra of V_2O_5–MoO_3/TiO_2 catalysts, and due to the higher sensitivity of this technique with respect to FT-IR and FT-laser Raman, information concerning the V species could be derived also from the samples with the lowest V content. Preliminary quantitative evaluation by EPR indicates that up to 10% of the total V + Mo in the ternary samples is present as V(IV) + Mo(V), which appears enough to adequately probe the structural features of the reduced ions anchored at the surface of the support. In line with the FT-IR data, EPR provided evidence on the fact that vanadium is present on the titania surface as vanadylic ions $(VO)^{2+}$ in axial symmetry. Two similar V(IV) species have been detected, slightly differing in their coordinative environment. A comparison with literature data indicates that these species are strictly similar to those observed in the case of V_2O_5–WO_3/TiO_2 (6) catalysts: the similarity of the EPR vanadium spectral features for the ternary systems containing tungsten or molybdenum oxide nicely indicates that these catalysts can be thought of as supported oxides where the main interaction is between the V_2O_5 supported phase and the TiO_2 support, while the interaction between the cosupported phases (V_2O_5–MoO_3 or V_2O_5–WO_3) is certainly weaker. However, a comparison of the simulations of the EPR spectra performed in the case of the binary V_2O_5/TiO_2 catalysts (6) also indicates that the spectroscopic features of the vanadyl ions present over the ternary V_2O_5–MoO_3/TiO_2 catalysts slightly differs with respect to those of V_2O_5/TiO_2. Indeed only one of the two families of VO^{2+} ions present in the ternary samples has been observed over the binary V_2O_5/TiO_2 catalysts. Furthermore, while the presence of V(IV) ions is observed over V_2O_5–MoO_3/TiO_2 catalysts already at R.T. after calcination in air, in the case of the V_2O_5/TiO_2 reference system the typical vanadium EPR spectrum is visible only in the case of the reduced samples, or it appears upon annealing at high temperatures (6). This indicates that in spite of the strong interaction between the V_2O_5 supported phase and the TiO_2 support, MoO_3 plays a role in determining both the amounts and the features of the surface reduced vanadyl ions in the V_2O_5–MoO_3/TiO_2 catalysts.

As opposed to the analogous V_2O_5–WO_3/TiO_2 system, where the presence of paramagnetic W(V) ions has never been observed in our previous studies (6), the existence of Mo(V) ions is clearly visible in the EPR spectra of the investigated V_2O_5–MoO_3/TiO_2 catalysts. Two similar but distinct species of Mo(V) ions have been observed, corresponding to molybdenylic ions in axial symmetry with slightly different coordinative environment. The Mo(V) species are strictly similar to those observed in the case of MoO_3/TiO_2 catalysts (9), again confirming that the features of the supported Mo phase are primarily governed by the interaction with the support. In line with the data coming from the vibrational spectroscopies, no evidence for the presence of polymeric molybdenum (V) clustered species have been provided by EPR.

In conclusion, spectroscopic data show that the characteristics of the V and Mo surface species are primarily determined by their interaction with the TiO_2 surface, and this calls for a structural and vibrational independence of the supported V and Mo oxide species. However, data presented in this work also suggest that, in spite of their structural independence, a specific electronic interaction does exist between the V and Mo surface oxide species that affects their characteristics. Indeed it was found that: (i) the V_2O_5 loading affects the intensities of both the vanadium and the molybdenum EPR signals (compare Figs. 3 and 4), i.e., it alters the reducibility of both V and Mo oxide species; (ii) the EPR spectral features of the surface vanadyl ions in the V_2O_5–MoO_3/TiO_2 system differ from those of the binary V_2O_5/TiO_2 samples, i.e., the presence of MoO_3 affects the characteristics of the V surface oxide species; (iii) the increase of the V_2O_5 loading broadens the EPR spectra, thus suggesting the presence of a sort of mutual interaction between supported paramagnetic species; (iv) vanadium addition to MoO_3/TiO_2 leads to an increase of the Raman scattering baseline likely due to an increase of the amount of quasi-free electrons in the samples, i.e., V modifies the sample reducibility. These observations converge in indicating the existence of a mutual electronic interaction between the V and Mo surface oxide species, as already suggested between V and W in the V_2O_5–WO_3/TiO_2 system (6). The suggested electronic interaction may operate via the conduction band of TiO_2, as already suggested between V and W in the V_2O_5–WO_3/TiO_2 system (6, 34), or may involve the presence of mixed V–Mo surface species for which evidence has not been provided by the characterization techniques but whose presence cannot be ruled out on the basis of the available data. The electronic interactions between the V and Mo supported oxide species

lead to a modification of the catalyst redox behavior, as reported in a companion paper (46).

Surface Acid Characteristics of V_2O_5–MoO_3/TiO_2 Catalysts

The catalyst surface of all the investigated samples is characterized by strong acidity, probed by NH_3-TPD and FT-IR studies of NH_3 adsorption. NH_3 adsorbs on the catalyst surface as ammonia coordinatively held over Lewis acid sites (bands at 1604 and near 1240 cm^{-1} with shoulders at 1255, 1225, and 1191 cm^{-1}) and as ammonium ions produced by ammonia protonation (bands at 1668 and 1448 cm^{-1}). NH_4^+ species are thermally less stable than molecularly coordinated NH_3 species, as pointed out by the spectra recorded upon outgassing the samples at increasing temperatures.

Vanadyls and molybdenyls act as adsorption sites for ammonia, as indicated by the perturbations induced on the first overtone of the V=O and Mo=O stretching modes. Ti^{4+} ions may also coordinate ammonia, as previously reported (42). NH_3 coordinated on Lewis sites is associated with Ti, V, and Mo oxide surface species, whereas Brønsted acid sites are absent on the surface of the pure titania (42) and originate from Mo–OH or V–OH oxide species. Note that Brønsted acidity is also observed over the surface of bulk MoO_3 (47) and of polycrystalline vanadia (48). Accordingly, the addition of both molybdenum and vanadium causes an increase of the number of the Brønsted sites. Moreover, as previously observed (19), molybdenum addition causes an higher increase of the strength of the Lewis acid sites with respect to the vanadium addition. The loading of vanadium in $MoO_3(6)/TiO_2$ catalyst does not change significantly the strength of the Lewis acid sites, although the formation of a new site, corresponding to a band near 1225 cm^{-1}, could be not excluded. Hence, the Lewis acid strength of the support is enhanced by Mo loading, and less by V addition. This can be interpreted assuming a different inductive effect of Mo oxide species on the nearest Ti^{4+} cations, which also act as Lewis acid sites.

Reactivity of V_2O_5–MoO_3/TiO_2 Catalysts in the Selective Catalytic Reduction of NO by NH_3

The ternary V_2O_5–MoO_3/TiO_2 catalysts investigated in the present study exhibit a higher reactivity in the SCR reaction with respect to binary V_2O_5/TiO_2 and MoO_3/TiO_2 samples having the same metal oxide loading, and this may suggest that a synergistic effect operates between the V and Mo surface oxide species. To better analyze such aspects, following the kinetic analysis already proposed in the case of the V_2O_5–WO_3/TiO_2 catalysts (5, 6), the reactivity of V and Mo surface species has been estimated in the binary V_2O_5/TiO_2 and MoO_3/TiO_2 catalysts and then compared with that of V and Mo in the ternary V_2O_5–MoO_3/TiO_2 catalysts. For this purpose, the V and Mo turnover frequencies (TOF_V and TOF_{Mo}, respectively) in the binary V_2O_5/TiO_2 and MoO_3/TiO_2 systems have been calculated first. By assuming that all the Mo and V atoms are dispersed on the TiO_2 surface (and hence accessible to the reactants), and by taking into account the reactivity of exposed Ti atoms on the NO consumption, the following equation can be used for the evaluation of the TOF values,

$$TOF_M = r_{NO} - TOF_{Ti} \cdot \frac{mol_{Ti}}{g_{cat}} \Big/ \frac{mol_M}{g_{cat}} \qquad [2]$$

where M stands for V or Mo, r_{NO} is the NO consumption rate calculated from the values of k^0 and E_{act}, mol_M is the moles of V or Mo estimated from the nominal V and Mo loading, respectively, and mol_{Ti} is the moles of Ti exposed on the surface estimated from the values of A_s and θ_{Ti} (Table 1) and by assuming that the area occupied by a Ti atom is 19 $Å^2$ (41). TOF_{Ti} is the TiO_2 turnover frequency estimated from catalytic activity data collected over the pure TiO_2 support (9).

The values of TOF_V and TOF_{Mo} estimated at 500, 550, and 600 K in V_2O_5/TiO_2 and MoO_3/TiO_2 binary samples, respectively, are reported in Table 3. The values of TOF_{Ti} obtained in the case of the pure TiO_2 support are also reported for comparison. It appears that the TOF_V values are higher than the TOF_{Mo} values, thus indicating the greater reactivity of vanadium if compared to molybdenum in the SCR reaction. The reactivity of Ti is, on the other hand, negligible at the investigated temperatures.

Once the V- and the Mo-TOF values have been secured, a theoretical rate of reaction R_{th} (moles NO converted s^{-1} g_{cat}^{-1}) for each ternary catalyst has been tentatively calculated according to the following additive model (5, 6):

$$R_{th} = TOF_V \cdot \frac{mol_V}{g_{cat}} + TOF_{Mo} \cdot \frac{mol_{Mo}}{g_{cat}} + TOF_{Ti} \cdot \frac{mol_{Ti}}{g_{cat}}. \qquad [3]$$

In Eq. [3] TOF_V and TOF_{Mo} are the TOFs of V and Mo in the V_2O_5/TiO_2 and MoO_3/TiO_2 binary samples having the same V and Mo loading of the selected ternary V_2O_5–MoO_3/TiO_2 catalyst. The estimates of R_{th} according

TABLE 3

Calculated Turnover Frequency (TOF, mol_{NO} converted s^{-1} mol_{Mo}^{-1} or mol_V^{-1}) for the Vanadia/Titania and the Molybdena/Titania Catalysts

Catalyst	Mo or V coverage	Ti–Mo–V turnover frequency (TOF)		
		500 K	550 K	600 K
TiO_2	—	0.12×10^{-6}	1.75×10^{-6}	15.50×10^{-6}
$MoO_3(6)/TiO_2$	0.63	1.29×10^{-4}	5.31×10^{-4}	17.0×10^{-4}
$V_2O_5(0.8)/TiO_2$	0.08	0.30×10^{-3}	1.34×10^{-3}	4.56×10^{-3}
$V_2O_5(1.5)/TiO_2$	0.16	1.45×10^{-3}	4.80×10^{-3}	12.86×10^{-3}

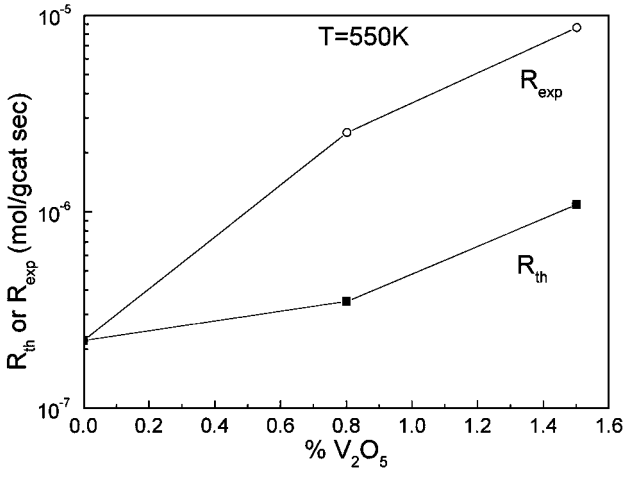

FIG. 11. Values of R_{th} and R_{exp} (moles NO converted s^{-1} g_{cat}^{-1}) for the $V_2O_5(x)$–$MoO_3(6)/TiO_2$ catalysts as a function of the V_2O_5 loading. $T = 550$ K; NO = 1000 ppm. Filled symbols, R_{th} values calculated according to Eq. [3]; open symbols, R_{exp} calculated from the estimated values of the activation energy and pre-exponential factor.

to Eq. [3] are based on the hypotheses that all the vanadium and molybdenum atoms loaded on the TiO_2 support are exposed at the surface and that their reactivity is equal to that of the corresponding binary samples having the same metal oxide loading.

The values of R_{th} estimated according to Eq. [3] for the investigated $V_2O_5(x)$–$MoO_3(6)/TiO_2$ catalysts at a selected temperature have been reported as a function of the V_2O_5 loading in Fig. 11 (open symbols) and compared with the corresponding experimental values (solid symbols). The figure shows that the values of the theoretical rate of reaction R_{th} estimated according to Eq. [3] are lower by one order of magnitude than those experimentally measured, R_{exp}. Hence, it may be argued that the reactivity of the V and/or Mo surface species in the ternary catalysts is higher than that of the same species in the binary samples having the same V_2O_5 and MoO_3 loading. This hints towards the existence of a synergism or interaction in the SCR reaction between the V and Mo supported metal oxide species.

It is worth noting that these results strictly parallel those previously reported for V_2O_5–WO_3/TiO_2 catalysts showing that the co-presence of W and V oxide on the TiO_2 surface greatly enhances the reactivity of the catalysts in the SCR reaction (4–6, 49). In such a case, the increase in the catalyst activity observed upon addition of WO_3 to vanadia/titania has been explained in several ways, including: (i) the formation of new Brønsted acid sites, considered the active sites in the SCR reaction (4); (ii) the formation of new acid sites that enhance the rate of reaction due to the requirement of a dual-site mechanism for the SCR reaction (49) or of an acid and a redox catalyst function (50); (iii) the increase of the catalyst redox properties due to the existence of a specific V–W interaction (5, 43, 51). The strict parallelism observed in terms of catalytic activity between the effects of MoO_3 and WO_3 addition to the V_2O_5/TiO_2 system likely suggests that the above-mentioned factors can be invoked to explain the observed increase of catalytic activity in the MoO_3-containing catalysts as well. As a matter of fact, the characterization data reported above clearly indicates that, like tungsten oxide, the addition of molybdenum to V_2O_5/TiO_2 increases the number of Brønsted acid sites and increases the strength of Lewis acid sites as well. This is in line with the hypothesis that the increase in the catalyst acidity is somehow responsible for the increase in the catalyst activity (4). However, our data also indicate that the loading of vanadium in $MoO_3(6)/TiO_2$ does not significantly change the acid characteristics of the catalysts (although the formation of a new acid site could be not excluded), whereas it greatly enhances the catalyst activity in the SCR reaction. Accordingly, it is unlikely that the catalyst activity is uniquely controlled by the catalyst acidity, either of Lewis or Brønsted type.

The hypothesis concerning the requirement of a dual-site mechanism for the SCR reaction or, similarly, of an acid and a redox function exploited by the Mo and V components, respectively, is in our opinion more likely. In this light, the increase in the catalyst activity that is observed upon addition of MoO_3 to V_2O_5/TiO_2 may be rationalized by considering that Mo provides a nearby acid site to vanadium and/or that MoO_3 increases the catalyst redox properties, which have been claimed as the controlling factor at low temperatures in the SCR reactions in the case of V_2O_5-based catalysts (52, 53). As a matter of fact, our characterization data reported above apparently point out the existence of electronic interactions involving the V and Mo oxide surface species leading to an increase of the redox characteristics of the samples. These observations have also been confirmed by specific investigations currently in progress in our laboratories on the redox properties of the V_2O_5–MoO_3/TiO_2 catalysts and on the role of such properties in the SCR reaction (46).

The TiO_2-supported V_2O_5–MoO_3 and V_2O_5–WO_3 catalysts investigated in this study and in previous works (5, 6) exhibit similar structural and morphological characteristics and a similar activity in the SCR reaction at low temperatures. However, the MoO_3-based catalysts show a higher propensity towards N_2O formation and a more pronounced decrease in NO conversion at high temperatures. N_2O represents an undesired byproduct of the reaction due to its greenhouse effects, and therefore its formation must be avoided. Hence, this apparently limits the use of MoO_3-based catalysts in the low temperature region with respect to the analogous WO_3-containing system. The selectivity data reported in Fig. 8B apparently suggests that N_2O formation must be mainly ascribed to the presence of MoO_3, in line with previous studies on MoO_3/TiO_2 (9) and on WO_3-based catalysts (6, 9). The study of the mechanisms leading

to the formation of N_2O is not the object of the present work; however, the results of transient reactivity experiments performed with $NH_3 + O_2$ and with $NH_3 + NO + O_2$ mixtures over a selected V_2O_5–MoO_3/TiO_2 sample (Fig. 10) suggest that NO is involved in the formation of nitrous oxide according to the stoichiometry of the so-called Non-Selective Catalytic Reduction (NSCR) process,

$$4\,NH_3 + 4\,NO + 3\,O_2 \rightarrow 4\,N_2O + 6\,H_2O. \qquad [4]$$

Indeed much lower amounts of N_2O have been obtained from $NH_3 + O_2$ mixtures in the absence of NO. These results are in line with the results of isotopic labeling experiments performed over vanadia/titania catalysts (54–59), showing that of the two N-atoms of N_2O one comes from ammonia and the other from NO, and with data obtained over binary MoO_3/TiO_2 catalysts as well (9). The occurrence of the direct ammonia oxidation to nitrous oxide (see below) cannot, however, be ruled out.

The reasons explaining the different extent of N_2O formation in the V_2O_5–MoO_3/TiO_2 and V_2O_5–WO_3/TiO_2 samples are still unclear. In the case of vanadia/titania samples, Bell and co-workers (52) associated the N_2O formation to the presence of labile oxygen atoms in polyvanadate species with respect to isolated vanadyls, i.e., to their superior redox properties. It is likely that a similar explanation holds for the investigated catalytic system as well. As a matter of fact, EPR data clearly point to the different redox properties of the molybdenyl vs the wolframyl surface species. Indeed, whereas Mo^{5+} ions were clearly detected in the case of the V_2O_5–MoO_3/TiO_2 samples, both after calcination at 773 K and/or after evacuation treatments at different temperatures, evidence for the presence of W^{5+} paramagnetic ions has never been collected either in the calcined samples or upon evacuation at increasing temperatures, up to 873 K (6, 9). These treatments certainly lead to the reduction of the catalyst, as visually indicated by the progressive darkening of the catalyst sample, but the lack of any W^{5+} EPR signal indicates the absence of stable W^{5+} ions. This clearly points out the different electronic characteristics of the MoO_3-based catalysts if compared to the analogous WO_3-containing samples. The role of these properties in determining the activity and selectivity in the reduction of NO is still unclear, but considering that the SCR reaction does involve a redox cycle it is expected that the different catalyst electronic properties play a role in governing the reactivity and selectivity of the different samples.

The decrease in the NO conversion that is observed at high temperatures over all the investigated $V_2O_5(x)$–$MoO_3(6)/TiO_2$ samples (Fig. 8) cannot be ascribed to the formation of N_2O via the NSCR reaction [4], which in fact does involve the same NH_3/NO ratio as the SCR reaction [1] and accordingly only affects the N_2 selectivity. Hence, other routes must be invoked, e.g., the ammonia oxidation reactions which have been proven to occur at high temperatures over the investigated catalytic system (see Fig. 10). The occurrence of these reactions, leading to the formation of NO and/or N_2O, is responsible for the decrease of both the NO conversion and the N_2 selectivity. On the other hand, when the reaction product is molecular nitrogen, only the NO conversion is affected (3). Hence, it may be speculated that the lower NO conversion observed at high temperature over V_2O_5–MoO_3/TiO_2 compared to V_2O_5–WO_3/TiO_2 may be ascribed to the lower reactivity of this latter catalytic system in the ammonia oxidation reaction.

Water addition has a significant beneficial effect on the catalytic behavior of the catalysts (see Fig. 10). Indeed the reactivity of the catalysts in the SCR reaction is only slightly decreased by the presence of water at low temperature (the NO conversion curve is slightly shifted towards higher temperatures), but higher NO conversions and N_2 selectivities are preserved at high temperatures. Accordingly water improves the catalyst performances by widening the temperature window of the SCR reaction towards higher temperatures. The beneficial effect of water on the catalytic performance of the V_2O_5–MoO_3/TiO_2 system is related to its weak inhibiting effect on the SCR reaction and to its simultaneous strong effect on the NH_3 oxidation reactions and/or nonselective NO reduction reaction. This is very evident in Figs. 9 and 10, showing that the NH_3 oxidation reactions are shifted roughly 100 K upwards by steam addition, whereas the SCR reaction is only weakly affected at low temperatures by the presence of water. The inhibiting effect of water on the SCR reaction is well established in the literature (1–3), and it has been interpreted in different ways, e.g., (i) competition of H_2O with NH_3 on the adsorption on the active sites, (ii) modification of the structure of the active sites (27, 60–67), and (iii) retention of high catalyst oxidation state (68). As a matter of fact, FT-IR data proved that water may convert Lewis acid sites into Brønsted ones (3), and this may result in a modification of the catalyst activity. Also, the improvement of the N_2 selectivity by water addition on V_2O_5/TiO_2 catalysts is well documented (69–72), but the mechanisms through which it exerts its inhibiting effects on N_2O formation are still rather obscure.

CONCLUSIONS

TiO_2-supported V_2O_5–MoO_3 oxide based catalysts, having V and Mo loadings representative of commercial SCR catalysts, have been considered in this study. Our data indicate that, in the range of compositions investigated (which are of interest for the SCR application), a strict parallelism does exist between the MoO_3- and the WO_3-based catalysts. Indeed these catalytic systems present similar structural and morphological properties, and, like WO_3, MoO_3

prevents the TiO_2 matrix sintering due to vanadia addition, thus acting as a "structural" promoter.

Molybdenum and vanadium oxide are present on the catalyst surface in the form of molybdenylic and vanadyl species, even if the presence of polymeric Mo_xO_y species cannot be excluded. The features of the V and Mo surface oxide species closely resemble those observed over the corresponding binary V_2O_5/TiO_2 and MoO_3/TiO_2 reference catalysts, thus pointing out the vibrational independence of the V and Mo surface species. Hence in these catalysts the main interaction is between the V_2O_5 and MoO_3 supported phase and the TiO_2 support, while the interaction between the co-supported phases (V_2O_5–MoO_3 or V_2O_5–WO_3) is certainly weaker. However, in spite of the structural and vibrational independence of the V and Mo surface species, electronic interactions between the TiO_2-supported V and Mo oxides are likely present. These interactions may operate via the TiO_2 support or may involve mixed V–Mo surface oxide species whose presence has not been observed but cannot be ruled out.

The catalyst surface of all the investigated samples is characterized by strong acidity, probed by NH_3-TPD and FT-IR. Ammonia is coordinatively held over Lewis acid sites (associated with Ti, V, and W oxide surface species) and is present as ammonium ions produced by NH_3 protonation over Mo–OH or V–OH oxide species. The addition of both molybdenum and vanadium causes an increase of the number of the Brønsted sites, and molybdenum addition also causes a higher increase of the strength of the Lewis acid sites with respect to the vanadium addition.

The V_2O_5–MoO_3/TiO_2 catalysts investigated in the present study exhibit an higher reactivity in the SCR reaction with respect to the corresponding binary V_2O_5/TiO_2 and MoO_3/TiO_2 samples having the same metal oxide loading. As a matter of fact, the temperature window for the SCR reaction, corresponding to high NO_x conversion and complete selectivity to N_2, is greatly widened with respect to the binary catalysts. Calculations showed that the reactivity of V and/or Mo in the ternary catalysts is higher than that of the same species measured in the case of V_2O_5/TiO_2 and MoO_3/TiO_2 binary samples: hence it is suggested that a synergism operates between the V and Mo surface oxide species. Accordingly molybdenum acts as a "chemical" promoter for the SCR reaction, besides playing a "structural" function as well. These results strictly parallel those obtained in the case of V_2O_5–WO_3/TiO_2 catalysts, where a cooperative effect has also been observed in the SCR reaction between the V and W supported oxide species. On the basis of the characterization data, it is suggested that the observed synergism in the SCR reaction is related to the existence of the V–Mo electronic interactions.

When compared to the V_2O_5–WO_3/TiO_2 catalysts, the V_2O_5–MoO_3/TiO_2 samples show similar activity in the reduction of NO by NH_3, but also lower selectivity (i.e., higher formation of N_2O) and lower NO conversions in the high temperature region. Our data suggest that the N_2O formation is mainly ascribed to a reaction between NO and NH_3 catalyzed by the MoO_3 component. Besides, the decrease in the NO conversion that is observed in the high temperature region can be associated to the occurrence of the ammonia oxidation reactions. Notably, water addition has a significant effect on the catalytic behavior of the catalysts, and in particular in the high-temperature region: indeed the presence of water preserves high NO conversions and high N_2 selectivities at the highest investigated temperatures with respect to the experiments performed under dry conditions. Accordingly, water improves the catalyst performance and widens the temperature window of the SCR reaction towards higher temperatures.

The different behavior of the V_2O_5–MoO_3/TiO_2 and V_2O_5–WO_3/TiO_2 samples is possibly associated with the different electronic characteristics of the MoO_3-based catalysts if compared to the analogous WO_3-containing samples. A detailed comparison of the catalytic properties of MoO_3- and WO_3-based model and commercial De-NO_x-SCR catalysts is presently under investigation, and results will be presented shortly.

REFERENCES

1. Bosch, H., and Janssen, F., *Catal. Today* **2**, 369 (1988).
2. Lietti, L., and Forzatti, P., *Heter. Chem. Rev.* **3**, 33 (1996).
3. Busca, G., Lietti, L., Ramis, G., and Berti, F., *Appl. Catal. B Environ.* **18**, 1 (1998).
4. Chen, J. P., and Yang, R. T., *Appl. Catal. A Gen.* **80**, 135 (1992).
5. Lietti, L., Forzatti, P., and Bregani, F., *Ind. Eng. Chem. Res.* **35**(11), 3884 (1996).
6. Alemany, L., Lietti, L., Ferlazzo, N., Forzatti, P., Busca, G., Giamello, E., and Bregani, F., *J. Catal.* **155**, 117 (1995).
7. Spitznagel, G. W., Huttenhofer, K., and Beer, J. K., *in* "Enviromental Catalysis" (J. N. Armor, Ed.), p. 172. Am. Chem. Soc., Washington, DC, 1994.
8. Ums, H., and Spitznagel, G. W., *in* "Div. Pet. Chem.," preprints, p. 130. Am. Chem. Soc., Washington, DC, 1994.
9. Nova, I., Lietti, L., Casagrande, L., Dall'Acqua, L., Giamello, E., and Forzatti, P., *Appl. Catal. B Environ.* **17**, 245 (1998).
10. Dyrek, K., Rokosz, A., and Madej, A., *Appl. Magn. Reson.* **6**, 309 (1994).
11. Bond, G. C., and Tahir, S. F., *Appl. Catal.* **71**, 1 (1991).
12. Ng, K. Y. S., and Gulari, E., *J.Catal.* **92**, 340 (1985).
13. Kim, D. S., Kurusu, Y., Wachs, I. E., Hardcastle, F. D., and Segawa, K., *J.Catal.* **120**, 325 (1989).
14. Ohsaka, T., Izumi, F., and Fujiki, Y., *J. Raman Spectrosc.* **7**, 321 (1978).
15. Stencel, J. M., *in* "Raman Spectroscopy for Catalysis," p. 185. Van Nostrand–Reinhold, New York, 1990.
16. Bond, G. C., Zurita, J. P., Flamerz, S., Gelling, P. J., Bosch, H., van Ommen, J. G., and Kip, B. J., *Appl. Catal.* **22**, 361 (1986).
17. Busca, G., Gallardo Amores, J. M., Piaggio, P., Ramis, G., and Sanchez Escribano, V., *J. Chem. Soc. Faraday Trans.* **90**, 3181 (1994).
18. Yi, L., Ramis, G., Busca, G., and Lorenzelli, V., *J. Mater. Chem.* **4**, 1755 (1994).
19. Del Arco, M., Martin, C., Ramis, G., Busca, G., and Lorenzelli, V., *J. Chem. Soc. Faraday Trans.* **89**(7), 1071 (1993).

20. Ramis, G., Busca, G., and Lorenzelli, V., *Z. Phys. Chem. Neue Folge* **153**, 189 (1987).
21. Vergnon, P., Bianchi, D., Benali Chaoni, R., and Condurier, G., *J. Chem. Phys.* **77**, 1043 (1980).
22. Ramis, G., Yi, L., and Busca, G., *Catal. Today* **28**, 373 (1996).
23. Ramis, G., Busca, G., Bregani, F., and Forzatti, P., *Appl. Catal.* **64**, 259 (1990).
24. Busca, G., and Marchetti, L., *J. Chem. Res. (S)*, 174 (1986).
25. Risiecka, M., Grzybowska, B., and Gasior, M., *Appl. Catal.* **10**, 101 (1984).
26. Busca, G., Marchetti, L., Centi, G., and Trifirò, F., *J. Chem. Soc. Faraday Trans. I* **81**, 1003 (1985).
27. Busca, G., Marchetti, L., Centi, G., and Trifirò, F., *Langmuir* **2**, 568 (1986).
28. Cavani, F., Centi, G., Foresti, E., Trifirò, F., and Busca, G., *J. Chem. Soc. Faraday Trans. I* **84**, 237 (1988).
29. Gallay, R., van der Klink, J. J., and Moser, J., *Phys. Rev. B* **34**, 3060 (1986).
30. Busca, G., and Giamello, E., *Mater. Chem. Phys.* **25**, 475 (1990).
31. Centi, G., Giamello, E., Pinelli, D., and Trifirò, F., *J. Catal.* **130**, 220 (1991).
32. Davidson, A., and Che, M., *J. Phys. Chem.* **96**, 9909 (1992).
33. Meriaudeau, P., Clerjaud, B., and Che, M., *J. Phys. Chem.* **87**, 3872 (1983).
34. Paganini, M. C., Dall'Acqua, L., Giamello, E., Lietti, L., Forzatti, P., and Busca, G., *J. Catal.* **166**, 195 (1997).
35. Pourbaix, M., "Atlas d'Equilibres Electrochimiques at 25°C." Gauthier-Villars, Paris, 1963.
36. Sazonova, N. N., Simakov, A. V., Nikoro, T. A., Barannik, G. B., Lyakhova, V. F., Zheivot, V. I., Ismagilov, Z. R., and Veringa, H., *React. Kinet. Catal. Lett.* **37**, 71 (1996).
37. Gallardo Amores, J. M., Sanchez Escribano, V., Ramis, G., and Busca, G., *Appl. Catal. B Environ.* **13**, 45 (1997).
38. Lin Vien, D., Colthup, N. B., Fateley, W. G., and Grasselli, J. G., *in* "The Handbook of Infrared and Raman Characteristic Frequencies of Organic Molecules." Academic Press, New York, 1991.
39. Laane, J., and Ohlsen, J. R., *Prog. Inorg. Chem.* **28**, 465 (1980).
40. Saur, O., Bensitel, M., Mohammed Saad, A. B., Lavalley, J. C., Tripp, C. P., and Morrow, B. A., *J. Catal.* **99**, 104 (1986).
41. Ramis, G., Busca, G., and Lorenzelli, V., *Z. Phys. Chim. Neue Folge* **153**, 189 (1987).
42. Ramis, G., Busca, G., Lorenzelli, V., and Forzatti, P., *Appl. Catal.* **64**, 243 (1990).
43. Marshneva, V. I., Slavinskaya, E. M., Kalinkina, O. V., Odegova, G. V., Moroz, E. M., Lavrova, G. V., and Salanov, A. N., *J. Catal.* **155**, 171 (1995).
44. Wong, W. C., and Nobe, K., *Ind. Eng. Chem. Prod. Res. Dev.* **23**, 564 (1984).
45. Ramis, G., Yi, L., Busca, G., Del Arco, M., Martin, C., Rives, V., and Sanchez Escribano, V., *Mater Chem. Phys.* **55**, 173 (1998).
46. Casagrande, L., Lietti, L., Nova, I., Forzatti, P., and Baiker, A., *Appl. Catal. B Environ.* **22**, 63 (1999).
47. Bianchi, D., Bernard, J. L., Camelot, M., Benali-Chaoui, R., and Teichner, S. J., *Bull. Soc. Chim. Fr.*, I-275 (1980).
48. Busca, G., Ramis, G., and Lorenzelli, V., *J. Mol. Catal.* **50**, 231 (1989).
49. Wachs, I. E., Deo, G., Weckhuysen, B. M., Andreini, A., Vuurman, M. A., de Boer, M., and Amiridis, M. D, *J. Catal.* **161**, 211 (1996).
50. Topsoe, N.-Y., Dumesic, J. A., and Topsoe, H., *J. Catal.* **151**, 241 (1995).
51. Lietti, L., Forzatti, P., and Berti, F., *Catal. Lett.* **41**, 35 (1996).
52. Went, G. T., Leu, Li-Jen, Rosin, R. R., and Bell, A. T., *J. Catal.* **134**, 492 (1992).
53. Lietti, L., and Forzatti, P., *J. Catal.* **147**, 241 (1994).
54. Janssen, F., Van den Kerkhof, F., Bosch, H., and Ross, J. J., *Phys. Chem.* **91**, 5931 (1987).
55. Janssen, F., Van den Kerkhof, F., Bosch, H., and Ross, J. J., *Phys. Chem.* **91**, 6633 (1987).
56. Duffy, B. L. D., Curry Hyde, H. E., Cant, N. W., and Nelson, P. F., *J. Phys. Chem.* **98**, 7153 (1994).
57. Ozkan, U. S., Cai, Y., and Kumthekar, M. W., *J. Catal.* **149**, 375 (1994).
58. Ozkan, U. S., Cai, Y., and Kumthekar, M. W., *J. Catal.* **149**, 390 (1994).
59. Ozkan, U. S., Cai, Y., and Kumthekar, M. W., *J. Phys. Chem.* **99**, 2363 (1995).
60. Busca, G., *Langmuir* **2**, 577 (1986).
61. Busca, G., *Mater. Chem. Phys.* **19**, 157 (1988).
62. Cristiani, C., Forzatti, P., and Busca, G., *J. Catal.* **116**, 586 (1990).
63. Ramis, G., Cristiani, C., Forzatti, P., and Busca, G., *J. Catal.* **124**, 574 (1990).
64. Eckert, H., and Wachs, I. E., *J. Phys. Chem.* **93**, 6796 (1989).
65. Wachs, I. E., *J. Catal.* **570**, 124 (1990).
66. Deo, G., and Wachs, I. E., *J. Catal.* **146**, 323 (1994).
67. Deo, G., and Wachs, I. E., *J. Catal.* **146**, 336 (1994).
68. Selim, S. A., Philip, Ch. A., and Mikhail, R., *Sh. Thermochim. Acta* **36**, 287 (1980).
69. Tufano, V., and Turco, M., *Appl. Catal. B Environ.* **2**, 9 (1993).
70. Turco, M., Lisi, L., Pirone, R., and Ciambelli, P., *Appl. Catal. B Environ.* **3**, 133 (1994).
71. Odenbrand, C. U. I., Gabrielsson, P. L. T., Brandin, J. G. M., and Andersson, L. A. H., *Appl. Catal.* **78**, 109 (1991).
72. Topsøe, N. Y., Slabiak, T., Clausen, B. S., Srnak, T. Z., and Dumesic, J. A., *J. Catal.* **134**, 742 (1992).